PNAS RESEARCH ARTICLE | EARTH, ATMOSPHERIC, AND PLANETARY SCIENCES OPEN ACCESS

Estimate of OH trends over one decade in North American cities

Qindan Zhu[a], Joshua L. Laughner[b], and Ronald C. Cohen[a,c,1]

Edited by Mark Thiemens, University of California San Diego, La Jolla, CA; received September 21, 2021; accepted February 18, 2022

The hydroxyl radical (OH) is the most important oxidant on global and local scales in the troposphere. Urban OH controls the removal rate of primary pollutants and triggers the production of ozone. Interannual trends of OH in urban areas are not well documented or understood due to the short lifetime and high spatial heterogeneity of OH. We utilize machine learning with observational inputs emphasizing satellite remote sensing observations to predict surface OH in 49 North American cities from 2005 to 2014. We observe changes in the summertime OH over one decade, with wide variation among different cities. In 2014, compared to the summertime OH in 2005, 3 cities show a significant increase of OH, whereas, in 27 cities, OH decreases in 2014. The year-to-year variation of OH is mapped to the decline of the NO_2 column. We conclude that these cities in this analysis are either in the NO_x-limited regime or at the transition from a NO_x suppressed regime to a NO_x-limited regime. The result emphasizes that, in the future, controlling NO_x emissions will be most effective in regulating the ozone pollution in these cities.

hydroxyl radical | ozone control | NO_x emission

Significance

OH is the critical chemical setting removal rates of local pollutants in the atmosphere. The importance of OH to tropospheric chemistry stands in stark contrast to the absence of long-term measurements. Here we synthesize a machine learning technique, satellite observations, and simulations from a state-of-the-art chemical model to estimate OH trends between 2005 and 2014 in 49 North American cities. Compared to the summertime OH in 2005, the OH in 2014 exhibits changes that range from −17 to +11% in different cities. The variation of OH over one decade can be explained by the chemical regime shifts over the years. The identification of chemical regime, in turn, sheds light on the effective policy for controlling ozone.

The hydroxyl radical (OH) is the dominant oxidant in the atmosphere. Reactions with OH initiate the chemistry of a variety of trace gases (1–3), including greenhouse gases such as methane (CH_4) and primary pollutants including carbon monoxide (CO), nitrogen dioxides (NO_x ($\equiv$ NO+NO_2)), and volatile organic compounds (VOCs). As a result, OH affects radiative forcing over a global scale and governs local pollution events over cities. In cities, the lifetime of the freshly emitted species is anticorrelated with the OH concentration (4). Laughner and Cohen (5) observe NO_x lifetime directly from space and conclude that significant shifts in the NO_x lifetime occurred between 2005 and 2014 among 30 North American cities, which, in turn, suggests an underlying variation in OH in these cities.

Moreover, OH defines the production of ozone (O_3) (6, 7). Ground-level ozone is a major secondary pollutant that leads to negative impacts on human health and triggers the risk of death from respiratory causes (8). Ozone exceeds health-based standards most often during summertime. Ozone results from reactions involving two predominant ozone precursors: NO_x and VOCs. In the presence of sunlight, OH oxidizes VOCs to form organic peroxy radicals (RO_2), and then RO_2 can react with NO to form NO_2 which photolyzes to produce O_3. Shown in Fig. 1, the ozone production rate $P(O_3)$ is a nonlinear function of both NO_x and VOCs, and its dependence on NO_x is similar to the dependence of OH on NO_x. Two distinct regimes are observed. At high VOC reactivity and low NO_x, both $P(O_3)$ and OH increase with enhancing NO_x, and the corresponding regime is identified by the limiting reagent as a NO_x-limited regime. In contrast, both $P(O_3)$ and OH show the opposite relationship with NO_x in the NO_x-saturated regime, which is characterized by high NO_x compared to VOC reactivity. In terms of reducing ozone pollution, the effectiveness of the emissions control strategy depends on whether the photochemical regime of ozone formation is a NO_x-saturated or NO_x-limited regime. Therefore, OH is the ideal target molecule to examine the chemical regime; the relationship between OH and NO_x at interannual time scales serves as an explicit proxy to monitor the shift of the chemical regimes.

Despite its pivotal role in oxidation chemistry, OH observations at urban or suburban areas are remarkably sparse. The longest record is reported in ref. 9 where continuous OH measurements were conducted at a rural site in southern Germany between 1999 and 2003. Other OH measurements, occurring either in situ or airborne, are limited to a shorter time scale ranging from days to months (10–17). The short lifetime (< 1 s) of OH, owing to the high reactivity, means local in situ chemistry dominates the OH budget. As a result, the high spatial heterogeneity makes it impossible to describe OH chemistry over a large spatial scale solely from in situ OH observations.

In a recent paper, we developed a machine learning (ML) model to represent the OH chemistry emphasizing urban areas (18). The model aims to represent the OH chemistry simulated from a state-of-the-art chemical transport model relying on a

Author affiliations: [a]Department of Earth and Planetary Science, University of California, Berkeley, CA 94704; [b]Division of Geological and Planetary Sciences, California Institute of Technology, Pasadena, CA 91125; and [c]Department of Chemistry, University of California, Berkeley, CA 94704

Author contributions: Q.Z., J.L.L., and R.C.C. designed research; Q.Z. performed research; Q.Z. and J.L.L. contributed new reagents/analytic tools; Q.Z. analyzed data; and Q.Z. wrote the paper.

The authors declare no competing interest.

This article is a PNAS Direct Submission.

[1]To whom correspondence may be addressed. Email: rccohen@berkeley.edu.

This article contains supporting information online at https://www.pnas.org/lookup/suppl/doi:10.1073/pnas.2117399119/-/DCSupplemental.

Published April 11, 2022.

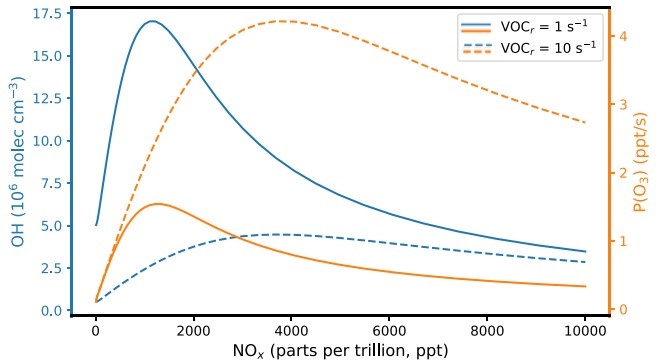

Fig. 1. A schematic of OH and $P(O_3)$ as a function of NO_x at the photochemical steady state. We assume a NO_2/NO ratio of 4, an alkyl nitrate branching ratio α of 0.04, and a HO_x production rate of 0.3 ppt×s^{-1}. Two scenarios represent a high VOC reactivity (VOC_r = 10 s^{-1}) condition and low VOC reactivity condition (VOC_r = 1 s^{-1}), respectively.

small set of observed constraints that are available with records over one decade. The ML model with observational inputs from satellite remote sensing yields estimates of surface OH across 49 North American cities for the time period of 2005–2014.

Variation of Urban OH over One Decade

The 49 selected cities exhibit a full range of variation in OH chemistry as characterized by the HCHO columns and NO_2 columns. Both HCHO columns and NO_2 columns are acquired from satellite-based observations and serve as indicators for VOCs (19–21) and NO_x (22, 23), respectively. We use the ratio of the HCHO column and the NO_2 column (satellite HCHO/NO_2) to reflect the relative availability of NO_x and total organic reactivity to hydroxyl radicals (24). Fig. 2 shows the ratio of average HCHO and NO_2 columns during April to September between 2005 and 2014 over selected cities. The satellite HCHO/NO_2 varies by a factor of 3, reflecting a range in NO_x and VOC chemistry. High satellite HCHO/NO_2 is indicative of an abundance of VOC relative to NO_x and presents in southeast US cities. It is consistent with VOC emissions mostly from biogenic sources, for instance, isoprene from vegetation (25). In contrast, the

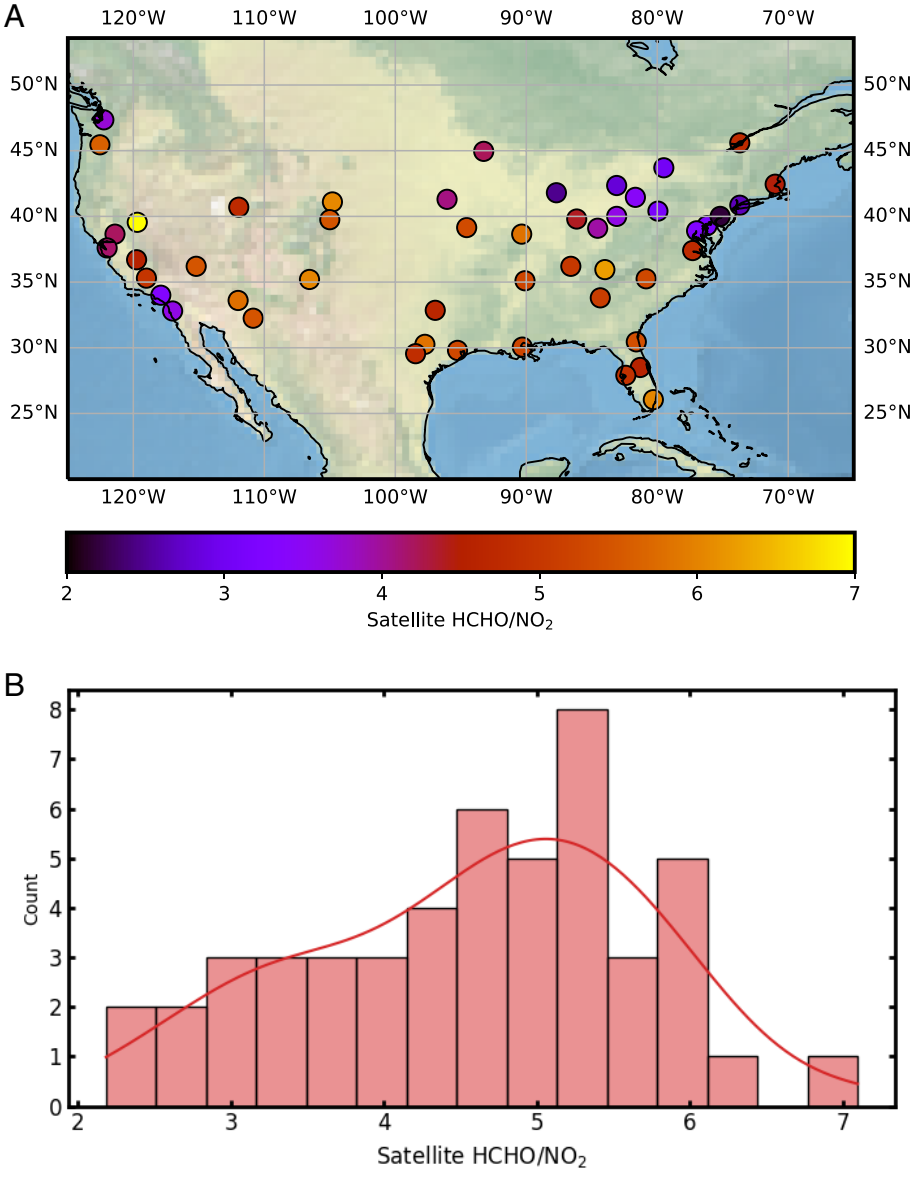

Fig. 2. The satellite HCHO/NO_2 over selected 49 cities. (*A*) The map of satellite-based summertime average of HCHO/NO_2 between 2005 and 2014 over 49 North American cities. (*B*) The frequency distribution of satellite HCHO/NO_2.

cities along the West Coast and the Northwest United States exhibit a relatively low satellite HCHO/NO_2 ratio. Those cities feature large anthropogenic NO_x emissions, whereas the VOC emissions are unreactive compared to the Southeast United States (26).

It also worth emphasizing the variation of the NO_2 and HCHO columns over one decade. Anthropogenic NO_x emissions exhibited a significant reduction over the United States due to stringent air pollution regulations during the 2005–2014 period. This is reflected in the decline in the satellite-observed NO_2 column. The selected cities include examples with the largest NO_2 column as well as the most pronounced reduction (*SI Appendix*, Fig. S1). The observed NO_2 column decreases by 33%, on average, over this time period. The largest decline of NO_2 column by up to 55% is observed in Los Angeles, followed by other populous cities including Chicago, Boston, and New York. Austin observes the smallest decrease, 11%. We also note the smaller decrease of the NO_2 column over urban regions in the central United States, which is thought to be partially due to the offset of increasing soil NO_x emission (27). Compared to the NO_2 column, HCHO columns show no consistent interannual variation (*SI Appendix*, Fig. S2). Among the selected cities, the relative change of HCHO column between 2005 and 2014 ranges from −15 to +10%. The causes of 10-y variation in the HCHO column are complex. While the anthropogenic VOC emissions from vehicles and industry declined (28), volatile chemical product emissions may be growing (29). Also, the changes in anthropogenic VOC emissions are masked by the large HCHO background driven by biogenic sources (30).

The interannual variation in both the NO_2 column and the HCHO column leads to variation in OH. Compared to summertime in 2005, the relative change of urban OH in 2014 ranges from −17 to +11% over the 49 cities (Fig. 3). We find that 30 cities show statistically significant changes in surface OH between 2005 and 2014. In four cities, including Los Angeles, New Orleans, New York, and Toronto, the increase of summertime averaged OH is larger than 4%. Thirty out of 49 cities witness a decline of annual OH in 2014 larger than −4%. Uncertainties are

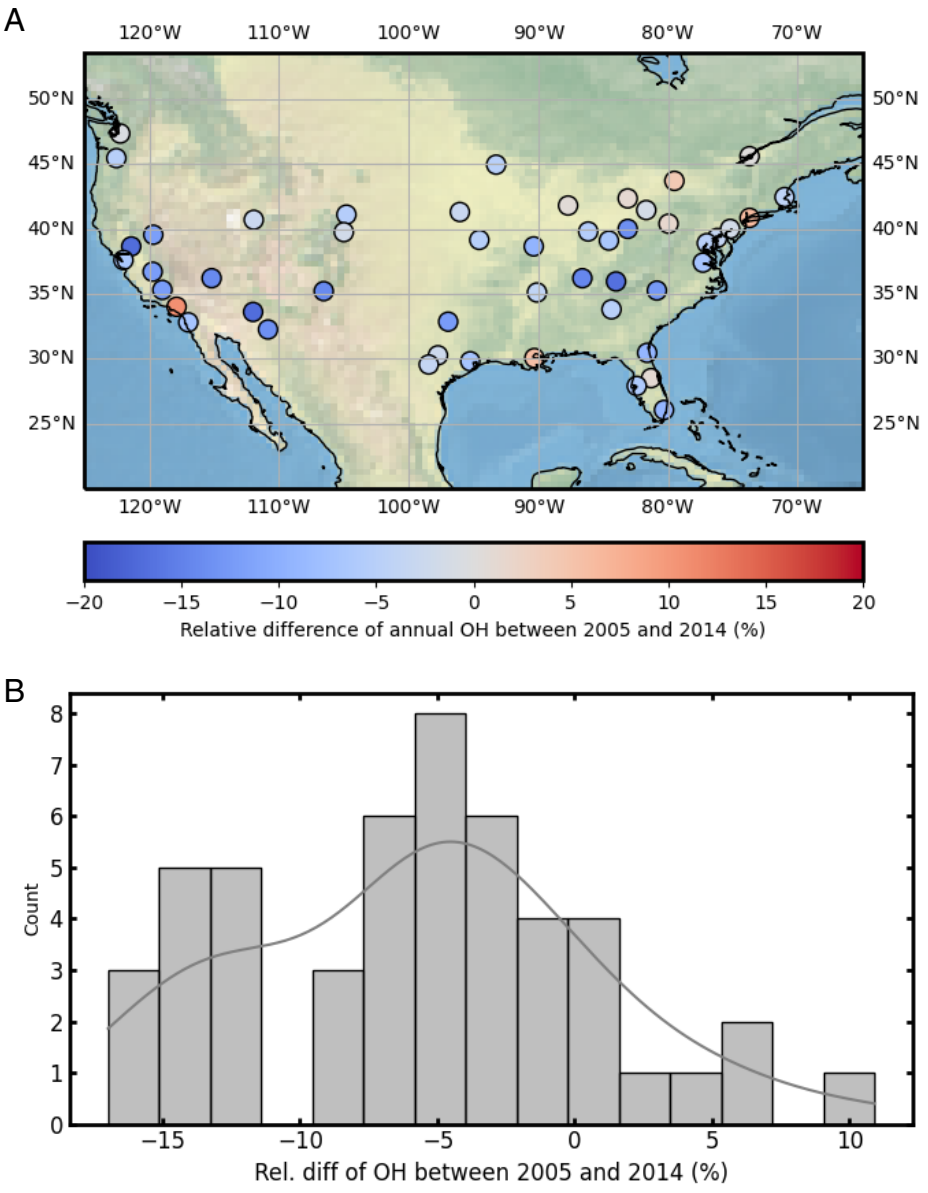

Fig. 3. The OH variation over selected 49 cities. (*A*) The map of the relative difference (Rel. diff) of summertime OH between 2005 and 2014 over 49 North American cities, and (*B*) the frequency distribution.

described in *Materials and Methods*. The full OH trends between 2005 and 2014 for each city are shown in *SI Appendix*, Fig. S3.

The Relationship between OH and NO_2 Column

Mapping the predicted OH to the concurrent NO_2 column depicts the relationship between OH and NO_x, and it reveals which chemical regime the urban environment falls in. For each city, we select the areas covering both city center and surrounding areas. If we assume that VOC reactivity is similar in all grids for a given urban area for a given year, the relationship between OH concentration and NO_2 column provides information about the dominant chemical regime. Assuming minimal variation in the VOC reactivity is supported by the small annual variation in HCHO shown in *SI Appendix*, Fig. S2 and similar weekend/weekday VOC reactivity observed in, for example, refs. 31–33.

Recall from Fig. 1 that the dependence of OH on NO_x is nonlinear, and the slope of OH vs. NO_x varies with its chemical regime. In the NO_x-saturated regime, OH is inversely correlated with NO_x, yielding a negative slope. The turnover point between the NO_x-saturated regime and NO_x-limited regime leads to a slope fluctuating around the zero point. Conversely, in the NO_x-limited regime, the slope is positive. The farther away from the turnover point, the larger the slope.

Fig. 4 shows how two cities, Los Angeles and Denver, illustrate different relationships between OH and NO_2 column and how it has shifted over the years. In 2005, Los Angeles was characterized by high NO_x (34). The average NO_2 column was 9.2×10^{15} molecules per cm^2, and the largest NO_2 column was 2.4×10^{16} molecules per cm^2. The OH from the ML model also shows a wide spread within the city, where OH concentration varies by a factor of 2. We note a significant inverse relationship; a higher NO_2 column corresponds to a lower OH concentration, yielding a slope of −0.1 (Fig. 4*A*). The observed slope matches the theoretical pattern of a NO_x-saturated regime as shown in Fig. 1. In contrast, Los Angeles in 2014 presented a much lower NO_2 column. The average NO_2 column is 60% lower than in 2005. Compared to the remarkable decline in the NO_2 column, the OH concentration shows a slight enhancement, 10% higher, on average, than those in 2005. As a consequence, the negative correlation between OH and the NO_2 column in 2005 vanishes.

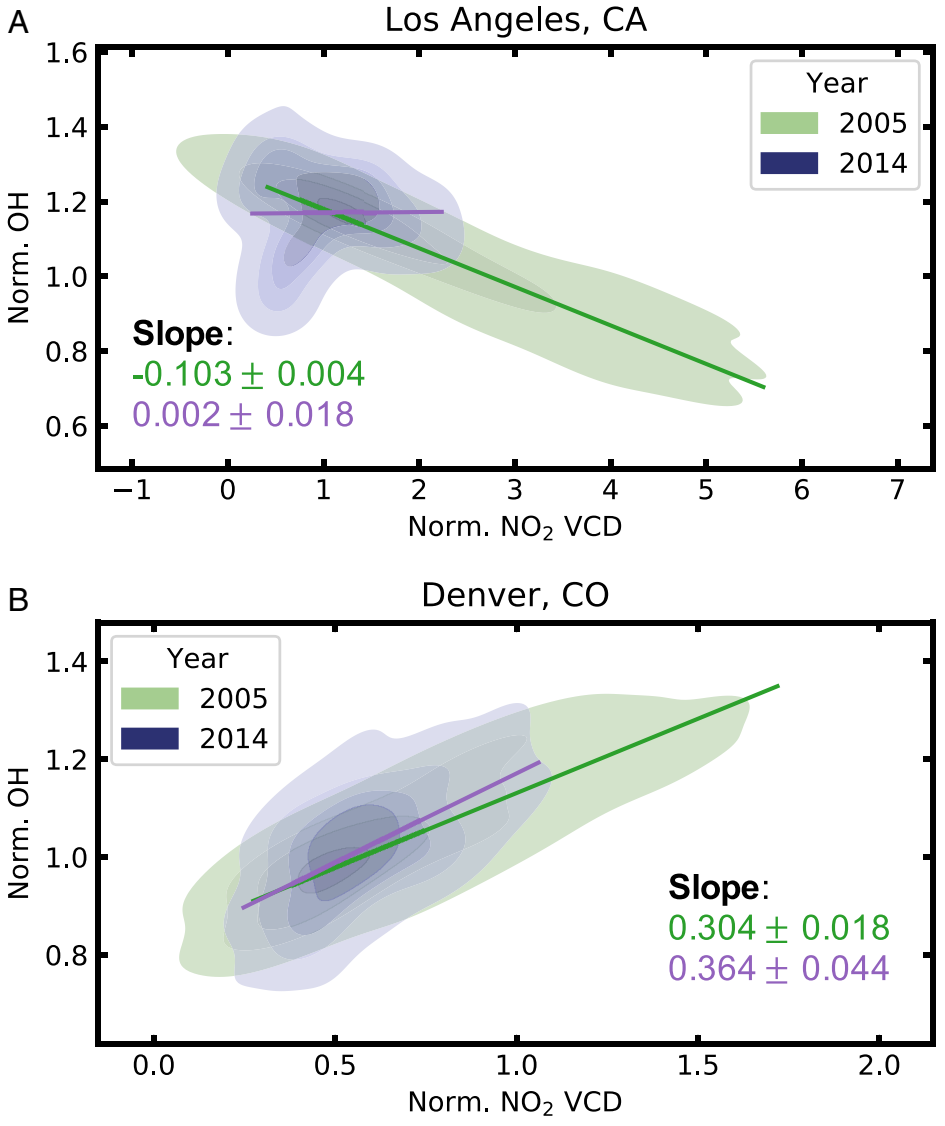

Fig. 4. The density plot between OH and the NO_2 column in 2005 and 2014 over (*A*) Los Angeles and (*B*) Denver. For each city, both OH and the NO_2 column are normalized to their annual averages in 2005. The lines and corresponding slopes denote the linear regression results between normalized OH and the normalized (Norm.) NO_2 column.

In 2014, OH presented a strong nonlinear dependence on the NO_2 column. Although a linear regression fails to describe the full pattern between OH and the NO_2 column, the slope from linear fitting shows a large fluctuation near the zero point, indicative of the turnover point between the NO_x-saturated regime and the NO_x-limited regime. Expanding the relationship analysis of OH and NO_2 column to each year between 2005 and 2014 shows a continuous increase of the slope, indicating a consistent transition from a NO_x-saturated regime (*SI Appendix*, Fig. S4).

In contrast, the OH–NO_2 column relationship in Denver indicates that NO_x-limited chemistry dominated the Denver plume between 2005 and 2014 (*SI Appendix*, Fig. S5), and Fig. 4*B* shows the OH–NO_2 column relationship in 2005 and 2014. In 2005, the NO_2 column was moderate compared to Los Angeles; the average NO_2 column was 2.8×10^{15} molecules per cm^2, and the largest NO_2 column was 7.2×10^{15} molecules per cm^2. A positive correlation between OH and the NO_2 column is observed, with a slope of 0.30. The slope of the correlation suggests Denver was already NO_x limited in 2005. In 2014, on average, there was a 16% decrease in the NO_2 column. However, the peak NO_2 column decreased by 36%, reflecting the effective emission control near the city center. The positive correlation between OH and NO_2 column continues in 2014, with its fitted slope increasing from 0.30 to 0.36. The enhancement in slope is consistent with, in 2014, moving farther away from the turnover point, along with the decline in the NO_2 column.

We extend the investigation of the relationship between OH and NO_2 column to 49 cities. In both 2005 and 2014, we conduct the linear regression between normalized OH and normalized NO_2 column; these slopes are summarized in Fig. 5, and the slopes for all years between 2005 and 2014 are shown in *SI Appendix*, Fig. S6. The year 2005 sees a wide scatter of the slope between normalized OH and normalized NO_2 column. Five cities, including New Orleans, Los Angeles, Tampa, and Boston, present a negative relationship between OH and NO_2 column. Sixteen cities yield a slope fluctuating around zero and a correlation coefficient (r^2) lower than 0.6. The rest of the cities observe strong positive correlations ($r^2 > 0.6$), with the slope larger than 0.2.

In 2014, the slopes in 45 out of 49 cities are more positive than they were in 2005. Cities such as Los Angeles have a negative slope closer to zero, indicating a transition from the NO_x-saturated regime to the turnover point of two regimes. Most cities whose slope is positive in 2005 increase further, demonstrating a shift within the NO_x-limited regime.

Implication for Controlling Ozone Pollution

In 2021, 50 areas and 196 counties are designated as ozone nonattainment areas where 8-h ozone levels fail to meet the National Ambient Air Quality Standards, affecting over 120 million people (35). Efforts devoted to reducing high ozone have focused on reduction of O_3 precursors emitted by anthropogenic sources. NO_x and VOC emission reductions have occurred (26, 36). However, the effectiveness of emission control on lowering ozone level encompasses a large variation and is associated with the chemical regime of the urban environment. In NO_x-saturated regime, NO_x emission reductions are detrimental to the mitigation of ozone pollution in the short term. In the NO_x-limited regime, there are immediate benefits. Based on our conclusion of the chemical regime shifts, most North American cities were NO_x limited in 2014. If further controls on NO_x emission are prioritized for regulating ozone, the regulations will likely be effective.

Conclusion

We leverage ML combined with satellite observations, to estimate surface OH in 49 cities. We found changes in the summertime OH between 2005 and 2014, ranging from a decrease of 17% to an enhancement of 11%. We observe a shift of chemical regimes, with a NO_x-limited regime now in effect in most cities. Thus, continued reduction of NO_x emissions will effectively control ozone.

Materials and Methods

The analysis code is available at https://doi.org/10.5281/zenodo.5296044 (37), and intermediate datasets are available at https://doi.org/10.6078/D1FM75 (38).

Observational and Model Records Used. All observational inputs are publicly available. We use observations from the Ozone Monitoring Instrument (OMI).j The NO_2 retrievals are from Version 3.0B of the Berkeley High Resolution (BEHR) OMI NO_2 product (https://behr.cchem.berkeley.edu/home/), and HCHO retrievals are from the Quality Assurance for Essential Climate Variables project

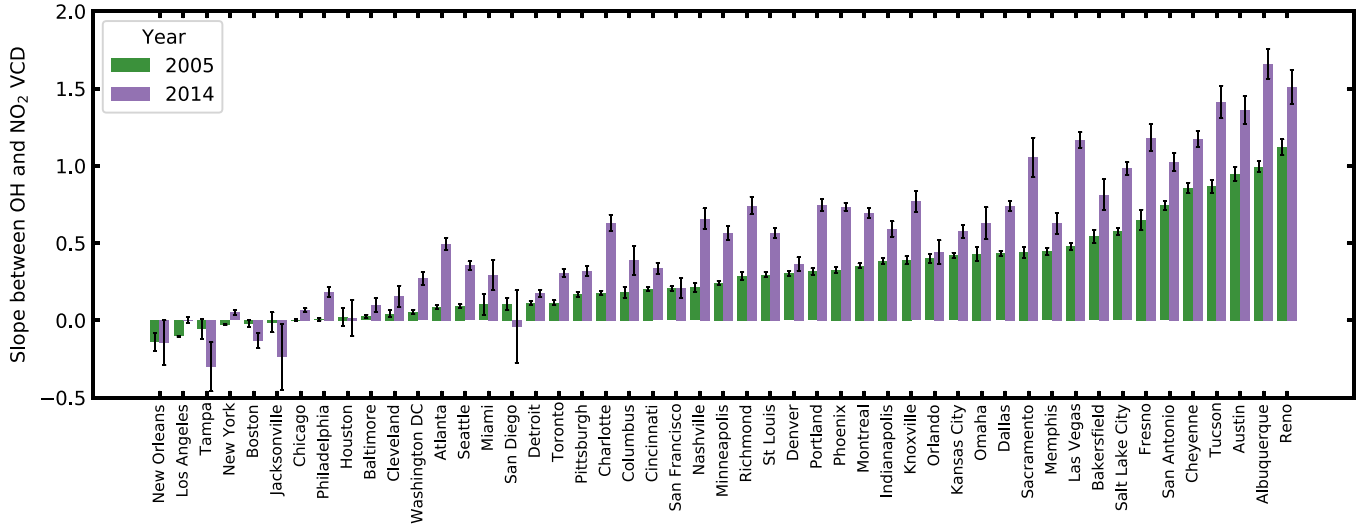

Fig. 5. The slope calculated from linear fitting between normalized OH and the normalized NO_2 column among 49 North American cities in both 2005 and 2014, same as Fig. 4. The error bar denotes the SD of the fitted slope.

(www.qa4ecv.eu). We conduct a start-of-art chemical transport model simulation using Weather Research and Forecasting Model coupled with Chemistry (WRF-Chem) over North America. Hourly outputs are sampled at the spatial resolution of 12 km × 12 km. The model configuration is described in detail in ref. 39.

ML Model. We utilize a gradient boosted tree model to represent the OH chemistry over urban areas during summertime. It is a supervised ML model and is optimized for predicting the surface OH by learning the training data.

We prepare training data solely from a chemical transport model, WRF-Chem. We use six parameters as predictors, including four surface variables ($J(O^1D)$, H_2O, temperature, and pressure) and two column variables (NO_2 column and HCHO column). The calculation of two column variables incorporates the averaging kernel from the satellite products to emulate the quantities observed from space, referring to section 7.4 of Laughner et al. (39). We select the WRF-Chem grids covering 49 North American cities, and each grid has a spatial scale of 12 km × 12 km. To represent each city, we select grid cells in a circular area with the radius varying from 0.5° to 1.0° around the city center based on the city size and the surrounding interference. The selection of 49 cities is consistent with Russell et al. (36) and Laughner and Cohen (5). We constrain the time to ∼13:30 local hour from April through September between 2005 and 2014 to present summertime conditions where the ozone pollution due to active photochemistry is most of a concern. For each city, we only filter out the days with lightning occurrence and with cloud fraction larger than 0.2.

Zhu et al. (18) evaluate the accuracy of this ML model and prove that the ML model using these six parameters is capable of capturing 76% of the OH variability and yields an RMSE of 2.1 × 10^6 molecules per cm^3. Therefore, the ML model serves as an efficient alternative to OH simulation using the computationally expensive chemical transport model.

OH Predictions. We combine model simulations and satellite observations to construct the observation-based inputs, and use the ML model to predict OH. Among the six features, we take $J(O^1D)$, H_2O, temperature, and pressure from the WRF-Chem outputs. Since meteorological parameters are constrained by the North American Regional Reanalysis every 3 h, we expect that these parameters are in good agreement with the observations. We use satellite retrievals described above to obtain both NO_2 column and HCHO column features. Based on the availability of OMI satellite observations and BEHR retrieval products that are optimized to remove bias on the spatial resolution of cities, we confine our study to 8 y between 2005 and 2014. OH predictions for years 2006 and 2010 are absent due to lack of WRF-Chem or BEHR retrievals.

Zhu et al. (18) calculate the uncertainty of the OH predictions. Besides those inherent in the ML model, the uncertainties from observed input parameters, especially the NO_2 column and the HCHO column, propagate through the ML model configuration and lead to nonnegligible influence on model performance. Considering the uncertainties of the retrievals products for both the NO_2 column and the HCHO column, we estimate the RMSE of OH predictions as 3.2 × 10^6 molecules per cm^3.

Summertime Average OH. We segregate the OH predictions by year and city, and then take the averages of grid cells per city per year to be representative of the summertime OH (Eq. **1**),

$$OH_{city,summer} = \frac{\sum_{day_i \subset summer} \sum_{grid_j \subset city} OH_{day_i,grid_j}}{\sum_{day_i \subset summer} 1 \times \sum_{grid_j \subset city} 1}. \quad [1]$$

The number of OH predictions used for calculation varies, as it depends on the number of grids for each city region as well as the number of valid days. The number of individual grid OH predictions ranges between 1,000 and 16,000. The minimum number corresponds to summertime OH in 2014 over Orlando, FL, which is consistent with a relatively small city size and fewer valid days in the analysis after filtering the days with lightning occurrence. We treat each OH prediction as an independent variable and use the lower bound of the number of observations; the RMSE of summertime average OH is 1.0 × 10^5 molecules per cm^3. It is a conservative estimate to compensate for the fact that the OH predictions are not perfectly orthogonal.

We then, for each city, assess the relative difference of summertime average OH between 2005 and 2014 (rel. OH hereinafter). The summertime average OH across all cities ranges from 8.7× 10^6 molecules per cm^3 to 1.33× 10^7 molecules per cm^3 in 2005, and ranges from 8.2× 10^6 molecules per cm^3 to 1.25× 10^7 molecules per cm^3 in 2014. Considering the estimate of RMSE of 1.0 × 10^5 molecules per cm^3, we calculate that the upper bound of the SD of rel. OH is 2%. Therefore, we take 4% as a threshold in the analysis; a rel. OH larger than 4% is considered statistically significant with 95% confidence.

Relationship between OH and NO_2 Column. To reconcile the large city-wise variation in both OH and the NO_2 column, both OH and the NO_2 column are normalized to their 2005 averages for a given city. We apply linear regressions to fit the normalized OH to the normalized NO_2 column and collect the slopes from the linear fitting. The shifts in slopes between OH and the NO_2 column are discussed in *The Relationship between OH and NO_2 Column*.

Data Availability. Zip data have been deposited in "Supporting data for 'Estimate of OH trends over one Decade in North American cities"' (https://doi.org/10.6078/D1FM75). The analysis code is available at Zenodo, https://doi.org/10.5281/zenodo.5296044 (37).

ACKNOWLEDGMENTS. We acknowledge support from NASA Grant 80NSSC19K0945. We acknowledge high-performance computing support from the Savio computational cluster resource provided by the Berkeley Research Computing program at the University of California, Berkeley (supported by the University of California, Berkeley Chancellor, Vice Chancellor for Research, and Chief Information Officer). We acknowledge use of the WRF-Chem preprocessor tools (boundary conditions using MOZART global model output, MOZBC) provided by the Atmospheric Chemistry Observations and Modeling laboratory of National Center for Atmospheric Research.

1. H. Levy 2nd, Normal atmosphere: Large radical and formaldehyde concentrations predicted. *Science* **173**, 141–143 (1971).
2. D. H. Ehhalt, Radical ideas. *Science* **279**, 1002–1003 (1998).
3. J. Lelieveld, F. Dentener, W. Peters, M. Krol, On the role of hydroxyl radicals in the self-cleansing capacity of the troposphere. *Atmos. Chem. Phys.* **4**, 2337–2344 (2004).
4. L. Valin, A. Russell, R. Cohen, Variations of oh radical in an urban plume inferred from NO_2 column measurements. *Geophys. Res. Lett.* **40**, 1856–1860 (2013).
5. J. L. Laughner, R. C. Cohen, Direct observation of changing NO_x lifetime in North American cities. *Science* **366**, 723–727 (2019).
6. J. Thornton *et al.*, Ozone production rates as a function of NOx abundances and HO_x production rates in the Nashville urban plume. *J. Geophys. Res. Atmos.* **107**, ACH-7-1–ACH-7-17 (2002).
7. D. Stone, L. K. Whalley, D. E. Heard, Tropospheric OH and HO_2 radicals: Field measurements and model comparisons. *Chem. Soc. Rev.* **41**, 6348–6404 (2012).
8. M. Jerrett *et al.*, Long-term ozone exposure and mortality. *N. Engl. J. Med.* **360**, 1085–1095 (2009).
9. F. Rohrer, H. Berresheim, Strong correlation between levels of tropospheric hydroxyl radicals and solar ultraviolet radiation. *Nature* **442**, 184–187 (2006).
10. K. Emmerson *et al.*, Urban atmospheric chemistry during the PUMA campaign 1: Comparison of modelled OH and HO_2 concentrations with measurements. *J. Atmos. Chem.* **52**, 143–164 (2005).
11. K. M. Emmerson *et al.*, Free radical modelling studies during the UK TORCH campaign in summer 2003. *Atmos. Chem. Phys.* **7**, 167–181 (2007).
12. X. Ren *et al.*, HOx concentrations and oh reactivity observations in New York City during PMTACS-NY2001. *Atmos. Environ.* **37**, 3627–3637 (2003).
13. Y. Kanaya *et al.*, Urban photochemistry in Central Tokyo: 1. Observed and modeled OH and HO_2 radical concentrations during the winter and summer of 2004. *J. Geophys. Res. Atmospheres* **112**, D21312 (2007).
14. S. M. Griffith *et al.*, Measurements of hydroxyl and hydroperoxy radicals during CalNex-LA: Model comparisons and radical budgets. *J. Geophys. Res. Atmos.* **121**, 4211–4232 (2016).
15. D. Sanchez *et al.*, Intercomparison of OH and OH reactivity measurements in a high isoprene and low NO environment during the Southern Oxidant and Aerosol Study (SOAS). *Atmos. Environ.* **174**, 227–236 (2018).
16. K. Lu *et al.*, Observation and modelling of OH and HO_2 concentrations in the Pearl River Delta 2006: A missing OH source in a VOC rich atmosphere. *Atmos. Chem. Phys.* **12**, 1541–1569 (2012).
17. K. Lu *et al.*, Missing OH source in a suburban environment near Beijing: Observed and modelled OH and HO_2 concentrations in summer 2006. *Atmos. Chem. Phys.* **13**, 1057–1080 (2013).
18. Q. Zhu, J. L. Laughner, R. C. Cohen, Combining machine learning and satellite observations to predict spatial and temporal variation of surface OH in North American cities. *Environ. Sci. Technol.*, 10.1021/acs.est.1c05636 (2022).
19. P. I. Palmer *et al.*, Mapping isoprene emissions over North America using formaldehyde column observations from space. *J. Geophys. Res. Atmos.* **108**, 4180 (2003).
20. T. M. Fu *et al.*, Space-based formaldehyde measurements as constraints on volatile organic compound emissions in East and South Asia and implications for ozone. *J. Geophys. Res. Atmos.* **112**, D06312 (2007).
21. D. Fu *et al.*, Direct retrieval of isoprene from satellite-based infrared measurements. *Nat. Commun.* **10**, 3811 (2019).
22. R. V. Martin, A. M. Fiore, A. Van Donkelaar, Space-based diagnosis of surface ozone sensitivity to anthropogenic emissions. *Geophys. Res. Lett.* **31**, L06120 (2004).
23. L. N. Lamsal *et al.*, Ground-level nitrogen dioxide concentrations inferred from the satellite-borne ozone monitoring instrument. *J. Geophys. Res. Atmos.* **113**, D16308 (2008).
24. S. Sillman, The use of NO_y, H_2O_2, and HNO_3 as indicators for ozone-NO_x-hydrocarbon sensitivity in urban locations. *J. Geophys. Res. Atmos.* **100**, 14175–14188 (1995).

25. A. Guenther *et al.*, Estimates of global terrestrial isoprene emissions using MEGAN (Model of Emissions of Gases and Aerosols from Nature). *Atmos. Chem. Phys.* **6**, 3181–3210 (2006).
26. S. Kharol *et al.*, Assessment of the magnitude and recent trends in satellite-derived ground-level nitrogen dioxide over North America. *Atmos. Environ.* **118**, 236–245 (2015).
27. G. Vinken, K. Boersma, J. Maasakkers, M. Adon, R. Martin, Worldwide biogenic soil NO_x emissions inferred from OMI NO_2 observations. *Atmos. Chem. Phys.* **14**, 10363–10381 (2014).
28. US Environmental Protection Agency, *Air pollutant emissions trends data 2016.* https://www.epa.gov/air-emissions-inventories/air-pollutant-emissions-trends-data. Accessed 23 March 2022.
29. B. C. McDonald *et al.*, Volatile chemical products emerging as largest petrochemical source of urban organic emissions. *Science* **359**, 760–764 (2018).
30. L. Zhu *et al.*, Long-term (2005–2014) trends in formaldehyde (HCHO) columns across North America as seen by the OMI satellite instrument: Evidence of changing emissions of volatile organic compounds. *Geophys. Res. Lett.* **44**, 7079–7086 (2017).
31. S. Beirle, U. Platt, M. Wenig, T. Wagner, Weekly cycle of NO_2 by GOME measurements: A signature of anthropogenic sources. *Atmos. Chem. Phys.* **3**, 2225–2232 (2003).
32. B. Kaynak, Y. Hu, R. Martin, C. Sioris, A. Russell, Comparison of weekly cycle of NO_2 satellite retrievals and NO_x emission inventories for the continental United States. *J. Geophys. Res. Atmospheres* **114**, D05302 (2009).
33. A. R. Russell, L. C. Valin, E. J. Bucsela, M. O. Wenig, R. C. Cohen, Space-based constraints on spatial and temporal patterns of NO_x emissions in California, 2005-2008. *Environ. Sci. Technol.* **44**, 3608–3615 (2010).
34. R. Gottlieb, R. Freer, M. Vallianatos, P. Dreier, *The Next Los Angeles: The Struggle for a Livable City* (University of California Press, 2006).
35. US Environmental Protection Agency, *8-hour ozone non-attainment areas (2015 standard).* https://www3.epa.gov/airquality/greenbook/jbtc.html. Accessed 15 August 2021.
36. A. R. Russell, L. C. Valin, R. C. Cohen, Trends in OMI NO_2 observations over the United States: Effects of emission control technology and the economic recession. *Atmos. Chem. Phys.* **12**, 12197–12209 (2012).
37. Q. Zhu, qdzhu/ml-pred-urban-oh: First release. Zenodo. https://zenodo.org/record/5296044#.YjtX_RDMKqU. Deposited 27 August 2021.
38. Q. Zhu, J. L., Laughner, R. C. Cohen, Supporting data for "Direct observation of changing NO_x lifetime in North American cities". Dryad. https://datadryad.org/stash/share/o6OCWYJeDj2Nv26h7I3vAfwa1PiAH7MAH743W76DwrY. Accessed 23 March 2022.
39. J. L. Laughner, Q. Zhu, R. C. Cohen, The Berkeley high resolution tropospheric NO_2 product. *Earth Syst. Sci. Data* **10**, 2069–2095 (2018).